ZULFAQAR Journal of Defence Science, Engineering & Technology
e-ISSN: 2773-5281
Vol. 5, Issue 1 (2022)
DOI: https://doi.org/10.58247/jdset-2022-0501-04
Journal homepage: https://zulfaqarjdset.upnm.edu.my

DETECTION OF VIBRATION FREQUENCY BASED ON NO CORE FIBER

Tee Kai Wen[a], Chew Sue Ping[b,*], Faiqahnor Abdul Latib[b], Latifah Sarah Supian[b]

[a] Department of MVS-VR-RD, ViTrox Technologies Sdn. Bhd., 14110 Penang, Malaysia
[b] Department of Electrical & Electronics Engineering, Faculty of Engineering, National Defence University of Malaysia, 57000 Kuala Lumpur, Malaysia

ARTICLE INFO

ARTICLE HISTORY
Received: 18-09-2021
Revised: 29-11-2021
Accepted: 18-02-2022
Published: 30-06-2022

KEYWORDS
No Core Fiber (NCF)
SNCS
Vibration frequency
Multimode interference

ABSTRACT

Vibration detection is an important feature in machinery health monitoring, in which used to detect faults and damages in heavy machines. This work demonstrated a fibre vibration sensor based on Single Mode-No Core-Single Mode (SNCS) fibre structure for low frequency vibration detection. When light coupled from Single-Mode-Fiber (SMF) to No-Core-Fiber (NCF), high-order Eigenmodes will be excited and caused interference between different modes occurred along NCF. Different vibration frequencies change the interference pattern inside the NCF as NCF acts as multimode waveguide. Two sets of SNCS sensor with different length of 1.65cm and 2.85cm obtained an average Electric Field Norm (EFN) losses of 5.242% and 9.233% respectively. The SNCS sensor was proven to be capable in detecting vibration frequencies ranging 100Hz to 3000Hz with vibration intensity of 3V and 5V. The maximum relative error of the vibration frequency is 7.32143×10^{-9}%. The SNCS structure has the advantage of easy to fabricate, low cost and immune to electromagnetic interference, which can be used in critical environment.

1.0 INTRODUCTION

Vibration sensor is utilized in many industries to help monitor trends of vibration levels in vital processes as well as machinery productions, which will simultaneously help the engineers to carryout suitable predictive and preventative maintenance programs to ensure smooth operations. Each industry normally needs a different vibration frequency with unique vibration patterns or signatures as part as its product traits. Different types of fibre sensor for vibration sensing have been proposed by other authors, employing Fabry-Perot Interferometer (FPI) [1], Long-period fibre grating [2], two- dimensional FBG [3], MEMS [4], distributed-feedback fibre laser [5], Mach-Zehnder [6], Butterfly-shaped Mach-Zehnder [7] and double fibre Bragg gratings (FBG) for multiple parameters sensing [8].

Recently, Lee et al. (2015) have developed an acoustic vibrations sensor based on Hollow Core Fiber (HCF). HCF is tapped in between two SMFs to form a rigid structure. Authors were able to detect vibration up to 10kHz with good Signal Noise Ratio (SNR) [9]. In other research, Wang et al. (2016) have proposed infrasound sensor based on Fabry-Perot Interferometer (FPI) structure. The transducer part of the sensor is composed of small round aluminium foil and polyethylene terephthalate film. Infrasound interference will caused the film to vibrate and changes the FPI cavity length [10]. A Stabilized FPI acoustic sensor have been proposed by Xuefeng et al. (2017) with improved wavelength tuning technique. Authors have introduced periodically wavelength tuning with distributed feedback laser and was able to detect minimum sound pressure level of 92mV/Pa [11]. Liu et al. (2015) also proposed a FPI sensor based on UV adhesive diaphragm to detect low acoustic frequency. Authors were able to detect frequency up to 20kHz with sensitivity of 57.3mV/Pa at 1000Hz [12].

*Corresponding Author | Chew, S. P. | sueping@upnm.edu.my

The Butterfly-Shape Mach-Zehnder Interferometer (BSMZI) was proposed by Zhao et al. (2018) for low-frequency vibration sensing, in which the sensing component is tapped at the hollow-core fibre (HCF) [13]. According to Zhao et al. (2018), it has a very low relative error in vibration frequency of less than 0.3% as well as a vibration measurement tolerance of 13.575dB/Watts with a range of 0 to 1 Watts under 50Hz vibration frequency. In addition, its marginal temperature tolerance ranges between 30°C to 70°C. The structure of this sensor allows it to provide a very high precision in frequency measurement with strong linearity of vibration sensing. Nevertheless, this structure also requires tapering which increases the production cost, complicates the structure as well as the difficulties in its fabrication process. Many works also found on different vibration sensor, such as combination of Single mode fibre (SMF) and Multimode fibre (MMF), which was presented [14]. This fibre vibration sensor was fabricated by etching the MMF that changes the self-imaging points (SIP) to a higher accuracy using the output connection of the SMF and MMF. It is observed that the SMS sensor had obtained high accuracy connection at SIP and was also sensitive towards vibration due to the etched MMF. The experiment was conducted using a 2cm long MMF, with an acoustic wave ranging from 20 to 300Hz. In addition, the sensitivity pressure is reported to be at 1.49mV/mPa with a linear correlation index of 0.9980 under vibration frequency of 120Hz.

Ma et al. (2015) carried out a numerical study on the fabrication of temperature sensor with thinner no core fibre (NCF) [15]. The work demonstrated a multimodal interference structure-based sensor with NCF. The author further claimed that the structure has a larger wavelength shift which is three-fold of the FBG based sensor. Another study conducted by Castillo-Guzman et al. (2010) on TEDFL (tuneable erbium-doped fibre laser) based on the MMI effects has suggested the usage of 4th self-imaging. In this study, the author utilised the MMI section as a noise filter. It is claimed that the 4th self-imaging mode was able to obtain the lowest insertion loss compared to other imaging modes. An SNR of 40dB with a wavelength range of 1549nm to 1609nm was obtained [16]. Geng et al. (2017) proposed a study on the refractive index sensor with temperature insensitive based on an NCF that is embedded with Long Period Grating (SNS LPG) [17]. Authors claimed that the SNS-LPG was able to exhibit high loss resonant dip up to 20dB. Thus, the sensitivity of the temperature and refractive index can be improved significantly as the author has managed to obtain an average wavelength sensitivity of 141.837 nm/RIU. Furthermore, a very low temperature sensitivity of (-6.43pm/°C) with high sensitivity of refractive index (RI) measurement of 141.837 nm/RIU were also obtained. Another similar work using NCF to detect broad range of frequencies due to vibration also found in [18-20]. Our work presents a fibre sensor based on NCF for low frequency vibration detection. Therefore, the objectives of this research are to investigate the working principle of SNCS sensor and fabrications of SNCS sensor for vibration detection. Besides that, accuracy and sensitivity performance of SNCS in detecting vibration frequency under impact of minimum temperature fluctuation is evaluated.

2.0 METHODOLOGY

2.1 Sensing Principle Of SNCS Vibration Sensor

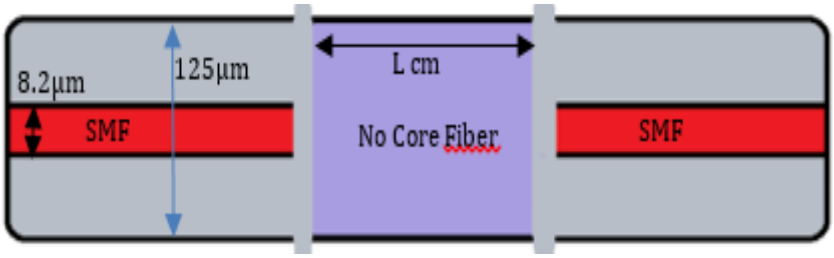

Figure 1. Schematic of SNCS Vibration Sensor

The schematic of the SNCS Vibration Sensor is illustrated in Figure 1. The main part of the sensor consists of input SMF1, NCF as sensing element and output SMF2. The working principle of the interference spectrum characteristics of the SNCS fibre sensor is explained using a two-beam interference model which is illustrated in Eqn. (1) and (2).

$$I_{out} = I_{mode1} + I_{mode2} + 2\sqrt{I_{mode1} I_{mode2}} \cos(\Delta\emptyset) \quad (1)$$

*Corresponding Author | Chew, S. P. | sueping@upnm.edu.my

Where I_{out} is the output light intensity, I_{mode1} and I_{mode2} are intensities of different modes, $\Delta\emptyset$ represent modal phase difference, which can be defined as

$$\Delta\emptyset = \frac{2\pi}{\lambda}\Delta nL = (2m+1)\pi \tag{2}$$

Where Δn is the effective refractive indices between the core mode and n^{th} order cladding modes. When light is transmitted from the SMF into NCF, high-order Eigen Modes is implemented while the light propagates along the NCF. The constructive interference wavelength between the 2 Eigen modes is expressed as:

$$\lambda_k = \frac{16n_{core^2k}}{(m-n)[2(m+n)-1]L} \tag{3}$$

Where L is the length, d represents the diameter, n_{core} represents refractive index of the NCF and k is integer m>n. Once the NCF under vibration condition, it will experience a photo-elastic effect which causes the refractive index profile to change, i.e. n_{core}. As a result, causing the output light intensity to continuously change as well. The changes in the wavelength between the 2 adjacent extremes are expressed as:

$$\Delta\lambda = \lambda_k - \lambda_{k-1} = \frac{16n_{core}d^2}{(m-n)[2(m+n)-1]L} \tag{4}$$

When the extreme condition in the environment (vibration, strain), the interference intensity will also change. This is because the desired output causes a larger change of intensity and dense (crests and troughs) on the interference spectrum. A simulation is conducted using COMSOL Multiphysics to study the optical field distribution across SNCS. The characteristics of SNCS sensor that used in the simulation are shown in Table 1. In the simulation, air will act as cladding of NCF with large different of refractive index. The light propagation of 1550nm wavelength across SNCS with 1.65cm NCF is shown in Figure 2. The simulation demonstrates re-imaging length within NCF at 1.65cm.

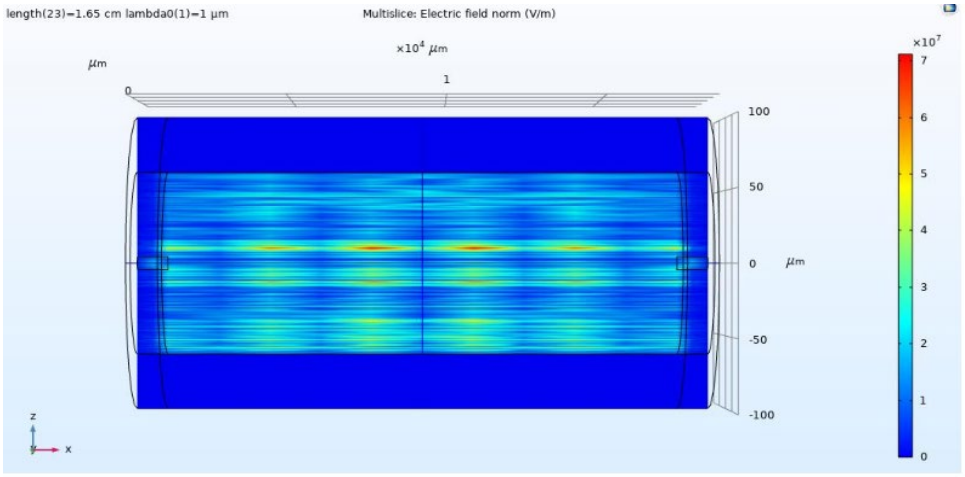

Figure 2. Light Propagation across SNCS sensor with NCF length of 1.65cm

Table 1. Characteristics of SNCS vibration sensor

n_{core} of SMF	1.550
$n_{cladding}$ of SMF	1.557
n of NCF	1.550
n of air	1.000
Cladding Diameter of SMF	125.0 µm
Core Diameter of SMF	8.250 µm
Diameter of NCF	125.0 µm
Wavelength of light source	1550 nm

*Corresponding Author | Chew, S. P. | sueping@upnm.edu.my

2.2 Fabrication Of SNCS Vibration Sensor

The fabrication process of the SNCS fibre sensor is divided into three main steps. Firstly, the fibres will be cut involving several processes such as striping, cleaving and cleaning processes. For NCF, the buffered jacket as well as cladding will be stripped thoroughly to increase its sensitivity towards the environment. However, for SMF, only approximately 3cm of its tip will be stripped. Sumitomo Electric cleaver (FC-6RM-C) was used to cleave them according to its desired length. The cleaved SMF and NCF fibres will be spliced using a conventional fusion splicer which utilises electric arc to melt the fibres, causing the two fibre ends to be permanently welded together. During this process, the fusion splicer module must be properly aligned. The splicer should weld both fibres together with minimal losses. Lastly, the NCF is measured and cleaved accordingly before it is spliced together with the SMF fibre to create a sandwich structure.

2.3 Experiment Setup For Vibration Testing

The schematic diagram of experimental setup is illustrated on Figure 3(a). The SNCS vibration sensor is attached to a beam. A signal generator is used to generate vibration signal using sine waveform. The desired frequency from 100Hz to 3000Hz and amplitude of 5V and 3V are set into the Signal Generator before a signal is sent to the vibration generator. The frequency response of the vibration generator encompasses the whole audio spectrum and beyond. The performance of the sensor is measured based on its sensitivity and accuracy through analysis and interpretation of the collected data. Relative error of the actual and desired frequency can be determined by obtaining the vibration frequency measurement of the piezoelectric accelerometer and the SNCS sensor which is essential to determine its accuracy. Meanwhile, the sensitivity of the sensor depends on the resolution of detectable vibration frequency. Frequencies ranged between 100Hz to 3000Hz is tested throughout the experiments.

The vibration input causes the beam structure to bend, causing the SNCS sensor to bend as well. This simultaneously causes multimode interference (MMI) distribution to occur. It is prompted by a change in the light coupled efficiency of the SNCS sensor. The frequency spectrum analyser will measure the vibration frequency as the vibration causes variations in power. For this experiment, the SNCS sensor is connected to the PD detector to detect the change of light intensity. It is then connected to an oscilloscope to observe the time domain response, with the vibration intensity acting as the constant variable. The overall experiment setup is illustrated in Figure 3(b). Vibration frequency can be easily obtained by applying the Fast Fourier Transform (FFT) to the time domain transmitted signals.

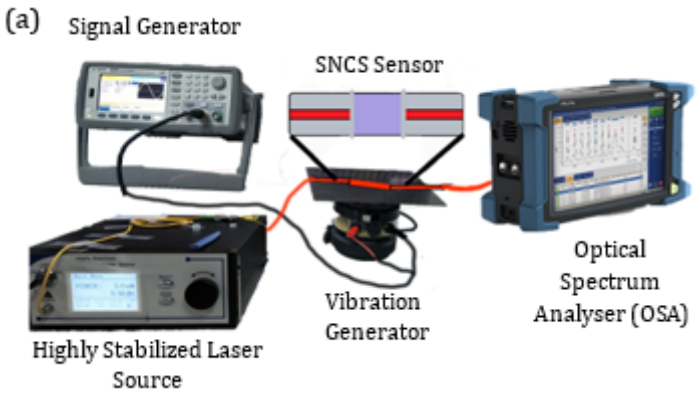

*Corresponding Author | Chew, S. P. | sueping@upnm.edu.my

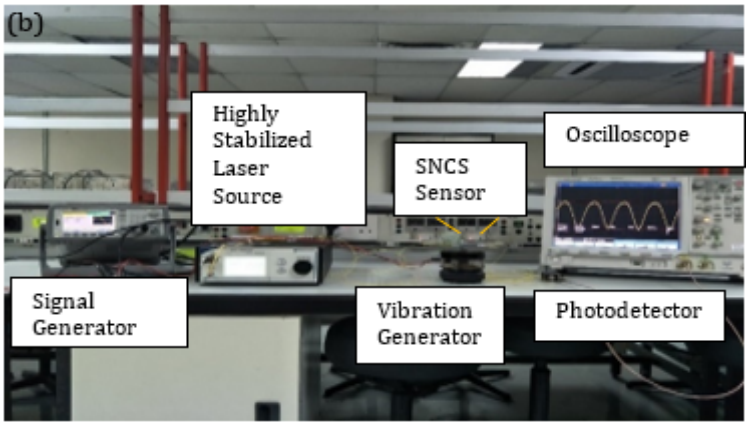

Figure 3. (a) Schematic diagram of experiment Setup for vibration intensity testing; and (b) Experiment Setup for vibration frequency testing

3.0 RESULTS AND DISCUSSION

3.1 Light Propagation Along SNCS Fiber Sensor

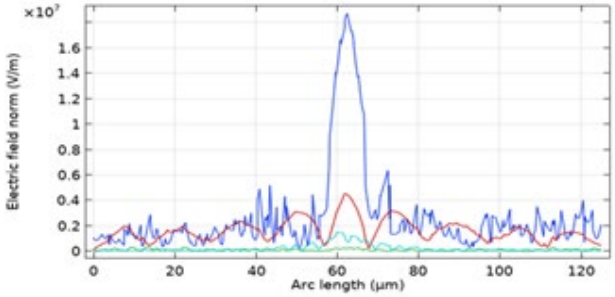

Figure 4. Graph of Electric field norm vs SMF Cladding Arc length of SNCS sensor at output NCF-SMF

Four sets of SNCS sensor with NCF length of 1.65cm, 1.90cm, 2.85cm and 5.75cm is being investigated on the losses of Electric Field Norm (EFN) when light is transmitted through NCF, as illustrated in Figure 4. COMSOL Multiphysics is used to simulate the optical distribution across SNCS sensor. The simulation indicates that at 1.65cm, 2.85cm and 5.75cm, re-imaging is formed. The re-imaging length within NCF demonstrate a lower percentage of EFN losses. However, when the length of re-image increases, the EFN peak losses increases by 11.55% per cm. The percentage of EFN losses is shown in Table 2.

Table 2. Table of the EFN average losses at the core of SNCS

Length(cm)	Peak EFN of SMF-NCF joint(V/m)	Peak EFN of NCF-SMF joint(V/m)	Losses of peak EFN(V/m)	Percentage of EFN Peak Losses (%)
1.65	19314164	19278182	35982	0.1863
1.90	6242305	295820	5946485	95.26
2.85	4709964	4532612	177353	3.766
5.75	4452400	1489808	2962592	66.54

In addition, as the length of the NCF increases, the losses of the optical power transmission increases. Re-image that is formed at the NCF-SMF joint allows the reduction of optical power transmission across the NCF which efficiently helps the propagation of light into SMF with minimum losses of power. However, as the number of re-image increases, the obtainable optical power transmission at the NCF-SMF joint decreases. Re-image that was formed at the NCF-SMF joint is crucial to ensure the efficiency of the optical power transmission. For further investigation, SNCS sensor with 1.65cm and 2.85cm NCF is fabricated for our experiments on sensitivity and accuracy of each SNCS sensor towards vibration frequency.

*Corresponding Author | Chew, S. P. | sueping@upnm.edu.my

3.2 Experiment of Low Frequency Vibration Sensing

An experiment is carried out to indicate the simulation result and observed the MMI of the SNCS sensor. When the beam is bent due to vibration signal, SNCS sensor is bend accordingly. Evanescent wave of high order modes that leaked out is enhanced due to the distribution of MMI. When the curvature increases, the characteristic wavelength of interference spectrum decreases. A SNCS sensor with 1.85cm NCF is fabricated to observe the transmission spectrum. Figure 5(a) shows the transmission spectrum of SNCS sensor based on vibration intensity modulation under 4V. The wavelength ranges of the interference range from 1520nm to 1570nm. Multiples dips and peaks can be observed from the transmission spectrum. The wavelength shifted to the right when the vibration intensity increases. This is due to the compressed and elongated of SNCS sensors when the intensity changes. The wavelength swift is almost linearly proportional to the vibration intensity. Figure 5(b) shows wavelength swift vs vibration intensity graph with R-square linear fitting of 0.8958.

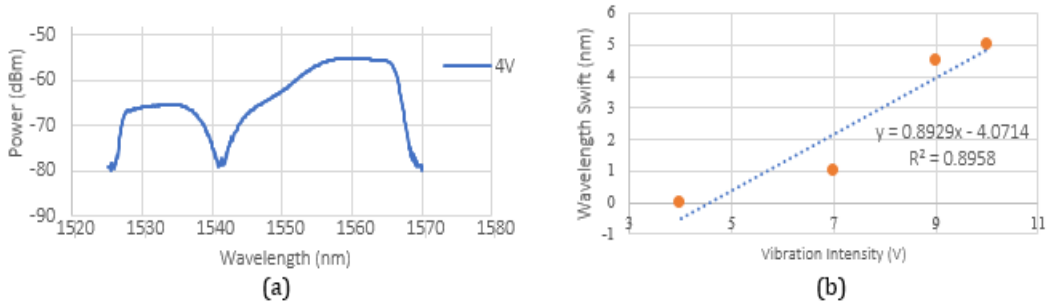

Figure 5. (a) SNCS transmission spectrum based on vibration intensity modulation under 4V vibration intensity; and (b) Graph of wavelength swift vs vibration intensity

During the experiment, signal generator generated a vibration signal which caused vibration platforms to vibrate. Hence, the beam that attached to vibration platform vibrates accordingly. SNCS sensor is also bent, which causes MMI. Thus, the light intensity is modulated by vibration signal. The sensing capability of SNCS sensor can be achieved by detecting the change of light intensity. Photodetector will help to convert the optical power into electrical power which changes as the vibration frequencies and intensities also changes. The power variation of the SNCS sensor is reflected by the photodetector through a real time monitoring using an oscilloscope to obtain the waveform data for vibration frequencies. Time domain graph of low frequency ranged between 100Hz to 3000Hz is detected under 5V vibration intensity. The time domain response is shown in Figure 6(a) and (b).

Based on the time response curve, it is found that the noise level varies for each different vibration frequencies. Thus, only frequency values with low level of noise can be obtained directly from the time domain curve. As the frequency increases, the period of waveform continues to become smaller. A fine and precise measurement is essential in obtaining an accurate frequency reading. Manually and directly harvesting frequency data from the time domain is impossible as the noise level and vibration frequency increases.

*Corresponding Author | Chew, S. P. | sueping@upnm.edu.my

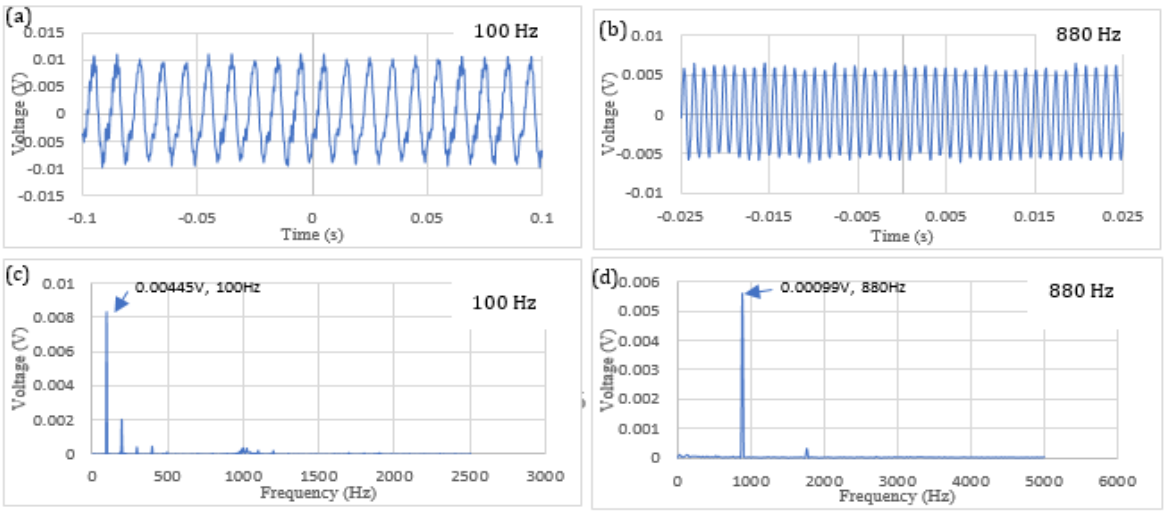

Figure 6. Time response curves of (a) 100Hz, (b) 880Hz; and Frequency response curves of (c) 100Hz, (d) 880Hz

Fast Fourier Transform (FFT) is then applied to the time domain to obtain the frequency of vibration signal. FFT is used to filter the noise from the vibration signal. The noise source is usually caused by the harmonic frequency. The harmonic frequency occurred due to a little axial misalignment between SNCS sensor and the vibration platform. Figure 6(c) and (d) shows the frequency response of 100Hz and 880Hz vibration frequency under 5V of vibration intensity. The amplitude of frequency domain represents the signal strength of each frequency. The higher the amplitude is, the higher the frequency strength becomes. Thus, noise can be eliminated through the FFT as the strongest frequency signal that can be observed directly from the frequency domain graph. Under 5V vibration intensity, SNCS sensor with 1.65cm NCF can detect low vibration frequency accurately. The maximum relative error is 7.32143×10^{-9}.

Next, the same method is conducted under vibration intensity of 3V. Figure 7(a) shows the comparison graph of measured frequency vs vibration frequency. The graph shows a linear fitting for both 5V and 3V vibration intensity using SNCS sensor with 1.65cm NCF. The maximum relative error for 3V intensity is 7.32143×10^{-9}, which is similar to 5V vibration intensity. Thus, SNCS sensor with 1.65cm NCF is sensitive to vibration signal and able to measure vibration frequency accurately. The linear fitting coefficient (R-squared) of SNCS sensor with 1.65cm NCF under 5V intensity is 0.9973, while the R-squared value is 0.9756 under 3V intensity. As the vibration intensity decreases, the R-squared value decreases. The SNCS sensor with 1.65cm NCF has the ability to measure vibration frequency accurately regardless of the vibration intensities. Moreover, the SNCS sensor with 1.65cm NCF is able to measure frequency accurately using low power laser source and low vibration intensity.

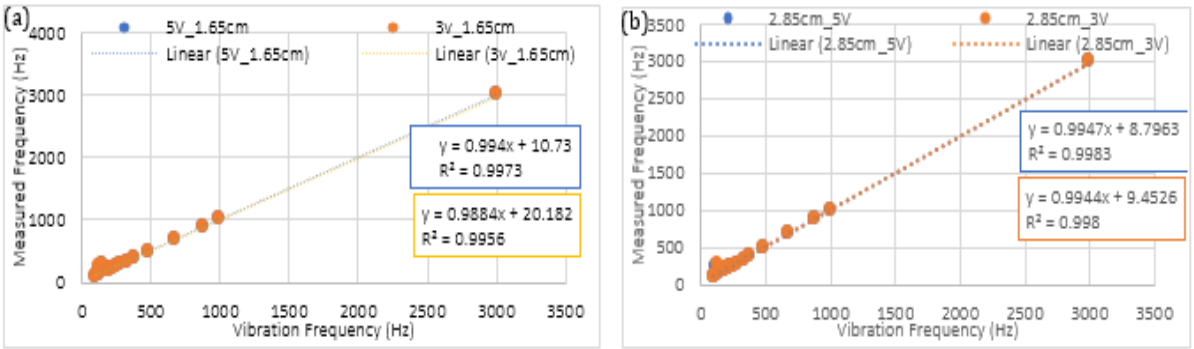

Figure 7. (a) Comparison graph of measured frequency vs vibration frequency for SNCS sensor with 1.65cm NCF; and (b) Comparison graph of measured frequency vs vibration frequency for SNCS sensor with 2.85cm NCF

Similar to the experiment of the SNCS sensor with 2.85cm NCF, two sets of experiment were carried out with the vibration intensity of 5V and 3V. Signal frequencies ranging from 100Hz to 3000Hz are

*Corresponding Author | Chew, S. P. | sueping@upnm.edu.my

utilized throughout the experiment. Figure 7(b) shows the comparison graph of measured frequency vs vibration frequency. Based on the figure, it is found that the trend line for the Measured Frequency versus Vibration Frequency graph for the 3V and 5V vibration frequency consist of a very small variation. The linear fitting coefficient (R-squared) is 0.9983 under 5V vibration intensity and 0.998 under 3V vibration intensity, which is approximately to 1. The maximum relative error for SNCS sensor with 2.85cm NCF under 5V and 3V vibration intensity is 7.32143 x 10^{-9}. The relationship of relative error and the vibration frequency is further studied. Figure 8(a) demonstrates the relative error for various vibration frequency for SNCS sensor with 1.65cm and 2.85cm NCF under 3V and 5V vibration intensity. It is observable that the relative error obtained are very low, which is less than 7.32143 x 10^{-9} when the vibration frequency is set from 100Hz to 3000Hz. The relative error increases as the vibration frequency increases. Therefore, for low frequency measurement, the SNCS sensor suited to obtain accurate result regardless of the vibration intensity.

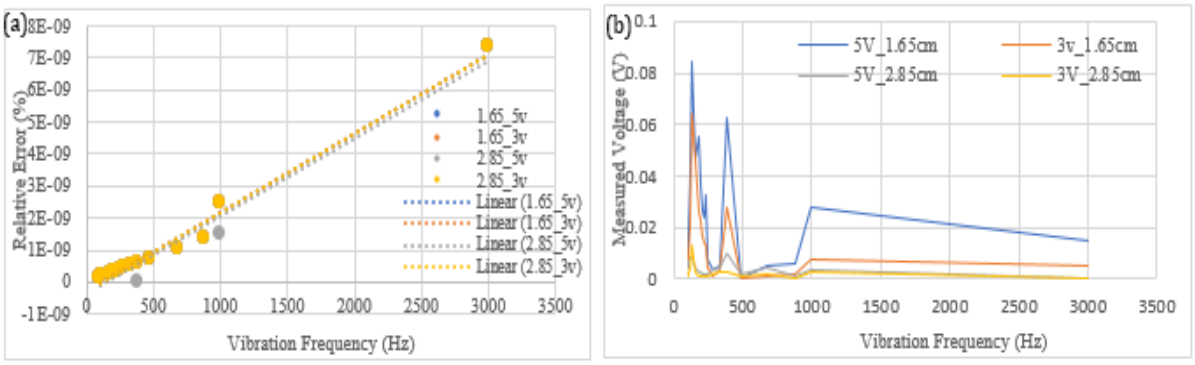

Figure 8. (a) Relative error vs vibration Frequency graph for SNCS sensor with 2.85cm NCF under 5V vibration intensity; and (b) Graph of measured voltage vs vibration frequency

When the low vibration frequency ranged from 100Hz to 1000Hz is measured, a linear trend line is detected and recorded for SNCS sensor with 1.65cm and 2.85cm NCF. Thus, for low vibration frequency measurement, a high accuracy of measured frequency is obtained regardless of its vibration intensity. It illustrates that the SNCS vibration sensor is able to sense vibration even with very low intensity as well as low power. Figure 8(b) shows the voltage variation along the vibration frequency. The maximum peak of measured voltage is the inherent frequency or the natural frequency of the beam that is attached to the vibration platform. It is caused by the resonance that occurred once the inherent frequency matches the vibration frequency, which also helps to provide a surged in the measured voltage. For each of the 4 sets of experiments, the maximum peak voltage is detected at 130Hz. Thus, 130Hz is regarded as the inherent frequency of the beam. It is deduced that the voltage will decrease once the vibration frequency increases. As a result, a higher amount of power or vibration intensity is required for high vibration frequency measurement. The average voltage for the SNCS sensor with 1.65cm NCF is six times higher than the SNCS sensor with 2.85cm NCF. The percentage of the Electric Field Norm at the NCF-SMF joint decreases as the length of NCF increases. Thus, the measured voltage of the SNCS sensor with 2.85cm NCF is considerably less compared to the SNCS sensor with 1.65cm NCF as there was more Electric Field losses along the NCF.

4.0 CONCLUSION

This work presents the experimental testing on a low-frequency vibration sensor based on Single Mode-No Core Fiber-Single Mode (SNCS). The sensory part of SNCS sensor is No Core Fiber (NCF), which is spliced in between two single mode fibre (SMF). Based on the finding, NCF of SNCS sensor was able to achieve least electric field norm (EFN) losses at 1.65cm, 2.85cm and 5.75cm as the re-image was successfully formed. When the length of NCF increases, the self-imaging replicant increases. The electric field norm losses increase by approximately 11.55% once the length of the NCF increases by 1cm. However, the effective interference length of NCF can only be obtained when the self-image is replicated at the NCF-SMF joint. The experiment has demonstrated that vibration frequency measurement using SNCS with 1.65cm and 2.85cm NCF. Vibration frequency measured by SNCS sensor is well matched with the applied frequency under vibration intensity of 3V and 5V. The linear fitting coefficient (R-squared) of measured frequency vs vibration frequency graph for all sets of experiment are more than 0.995. Besides, SNCS sensor was also able to achieve low relative error under vibration frequency range of

*Corresponding Author | Chew, S. P. | sueping@upnm.edu.my

100Hz to 3000Hz is obtained. Ergo, it can conclude that SNCS sensor able to achieve high accuracy and high sensitivity toward low vibration frequency.

5.0 ACKNOWLEDGEMENT

This work is supported by National Defence University of Malaysia under the short-term grant of UPNM/2019/GPJP/2/TK/7. The authors gratefully acknowledge the financial support provided.

List of Reference

[1] Zhao, Y., Chen, M., Xia, F., & Lv, R. (2018). "Small in-Fiber Fabry-Perot Low-Frequency Acoustic Pressure Sensor with PDMS Diaphragm Embedded in Hollow-Core Fiber," *Sensors Actuators A Phys.,* Vol. 270, pp. 162–169. doi: https://doi.org/10.1016/j.sna.2017.12.057.

[2] Zhang, Y. S., Zhang, W. G., Chen, L., Zhang, Y. X., Wang, S., Lin Yu, L., Li, Y. P., Geng, P. C., Yan, T. Y., Li, X. Y. & Kong, L. X. (2017) "Concave-Lens-Like Long-Period Fiber Grating Bidirectional High-Sensitivity Bending Sensor," *Opt. Lett.*, Vol. 42, No. 19, pp. 3892–3895. doi: 10.1364/OL.42.003892.

[3] Li, T., Tan, Y., Zhou, Z., & Wei, Q. (2015). "Pasted Type Distributed Two-Dimensional Fiber Bragg Grating Vibration Sensor," *Rev. Sci. Instrum.,* Vol. 86, No. 7, pp. 75009. doi: 10.1063/1.4927456.

[4] Liu, B., Lin, J., Ye, C., & Jin, P. (2016) "MEMS-Based High-Sensitivity Fabry–Perot Acoustic Sensor With a 45° Angled Fiber," *IEEE Photonics Technol. Lett.,* Vol. 28, No. 5, pp. 581–584. doi: 10.1109/LPT.2015.2506480.

[5] Liang, Y., Jin, L., Wang, L., Bai, X., Cheng, L., & Guan, B. O. (2017). "Fiber-Laser-Based Ultrasound Sensor for Photoacoustic Imaging," *Sci. Rep.,* Vol. 7, No. 1, pp. 40849. doi: 10.1038/srep40849.

[6] Kamenev, O. T., Kulchin, Y. N., Petrov, Y. S., Khiznyak, R. V., & Ramashko, R. V. (2016). "Fiber-Optic Seismometer on The Basis of Mach-Zehnder Interferometer," *Sensors Actuators, A Phys.,* Vol. 244, pp. 133–137. doi: 10.1016/j.sna.2016.04.006.

[7] Zhao, Y., Chen, M. Q., Xia, F., Cai, L., & Li, X. G. (2017). "Small Curvature Sensor Based on Butterfly-Shaped Mach-Zehnder Interferometer," *IEEE Trans. Electron Devices,* Vol. 64, No. 11, pp. 4644–4649. doi: 10.1109/TED.2017.2746087.

[8] Wang, J., Yu, Y., Chen, Y., Luo, H., & Meng, Z. (2015). "Research of A Double Fiber Bragg Gratings Vibration Sensor with Temperature and Cross Axis Insensitive," *Optik (Stuttg).,* Vol. 126, No. 7, pp. 749–753, 2015, doi: https://doi.org/10.1016/j.ijleo.2015.02.044.

[9] Lee, C., Tsai, Y., Chen, G., Xiao, Y., Hsu, J., & Horng, J. (2015). "Refined Bridging of Microfiber Plugs in Hollow Core Fiber for Sensing Acoustic Vibrations," *IEEE Photonics Technol. Lett.,* Vol. 27, No. 22, pp. 2403–2406, doi: 10.1109/LPT.2015.2466615.

[10] Wang, S., Lu, P., Liu, L., Liao, H., Sun, Y., Ni, W., Fu, X., Jiang, X., Liu, D., Zhang, J., Xu, H., Yao, Q., & Chen, Y. (2016) "An Infrasound Sensor Based on Extrinsic Fiber-Optic Fabry-Perot Interferometer Structure," *IEEE Photonics Technol. Lett.,* Vol. 28, No. 11, pp. 1264–1267. doi: 10.1109/LPT.2016.2538318.

[11] Mao, X., Yuan, S., Zheng, P., & Wang, X. (2017). "Stabilized Fiber-Optic Fabry-Perot Acoustic Sensor Based on Improved Wavelength Tuning Technique," *J. Light. Technol.,* Vol. 35, No. 11, pp. 2311–2314. doi: 10.1109/JLT.2017.2651151.

[12] Liu, L., Lu, P., Wang, S., Fu, X., Sun, Y., Liu, D., Zhang, J., Xu, H., & Yao, Q. (2016). "UV Adhesive Diaphragm-Based FPI Sensor for Very-Low-Frequency Acoustic Sensing," *IEEE Photonics J.,* Vol. 8, No. 1, pp. 1–9. doi: 10.1109/JPHOT.2015.2509866.

[13] Zhao, Y., Xia, F., Chen, M. Q., & Qing, L. R. (2018). "Optical Fiber Low-Frequency Vibration Sensor Based on Butterfly-Shape Mach-Zehnder Interferometer," *Sensors Actuators, A Phys.,* Vol. 273, pp. 107–112, 2018. doi: 10.1016/j.sna.2018.01.051.

[14] Gao, R., Wang, H., Zhu, D., Fan, G., Yan, H., Wang, P., Liu, Y., Wang, Y., Liu, W., Song, L., Wang, C., & Chen, Y. (2018) "Acoustic Frequency Vibration Sensor Based on Tapered SMS Fiber Structure," *Sensors Actuators, A Phys.,* Vol. 271, pp. 243–250. doi: 10.1016/j.sna.2018.01.023.

[15] Ma, L., Kang, Z., Qi, Y., & Jian, S., (2015). "Fiber-Optic Temperature Sensor Based on a Thinner No-Core Fiber," *Optik (Stuttg).,* Vol. 126, No. 9–10, pp. 1044–1046. doi: 10.1016/j.ijleo.2015.02.084.

[16] Castillo-Guzman, A., Antonio-Lopez, J. E., Selvas-Aguilar, R., May-Arrioja, D. A., Estudillo-Ayala, J., & LiKamWa, P. (2010). "Widely Tunable Erbium-Doped Fiber Laser based on Multimode Interference Effect," *Opt. Express,* Vol. 18, No. 2, pp. 591–597.

[17] Geng, T., Zhang, S., Peng, F., Yang, W., Sun, C., Chen, X., Zhou, Y., Hu, Q., & Yuan, L. (2017). "A Temperature-Insensitive Refractive Index Sensor Based on No-Core Fiber Embedded Long Period Grating," *J. Light. Technol.,* Vol. 35, No. 24, pp. 5391–5396. doi: 10.1109/JLT.2017.2772304.

*Corresponding Author | Chew, S. P. | sueping@upnm.edu.my

[18] Ran, Y., Xia, L., Han, L., Li, W., Rohollahnejad, J., Wen, Y., & Liu, D. (2015). "Vibration Fiber Sensors Based on SM-NC-SM Fiber Structure," *IEEE Photonics Journal*, Vol. 7, No. 2, pp. 1-7. doi: 10.1109/JPHOT.2015.2408436.

[19] A'qilah Ahmad Dahalan, Azali Saudi, & Jumat Sulaiman. (2020). "Path Finding Of Static Indoor Mobile Robot via AOR Iterative Method using Harmonic Potentials," *Zulfaqar Journal Of Defence Science, Engineering & Technology,* 3(2).

[20] Chew, S. P., Anis, S. N. M., Chi, Z. R., Wan Ariff Fadhil, W. A., Shee, H. C., Tee K. W., & Muhd Asran, T. (2022). "Faults Detection via Mobile Safety Inspection System," *Zulfaqar Journal of Defence Science, Engineering & Technology,* Vol. 4, No. 2.

*Corresponding Author | Chew, S. P. | sueping@upnm.edu.my